energies

MDPI

Article

Optimum Design of Large-Diameter Reverse Circulation Drill Bit for Drilling Rescue Wells Using Orthogonal Experimental Method and CFD Simulation

Kun Bo [1,2], Fangzhou Ji [1], Zhiqiang Zhao [3], Liming Fan [4] and Maosen Wang [1,2,*]

[1] College of Construction Engineering, Jilin University, Changchun 130021, China
[2] Key Laboratory of Drilling and Exploitation Technology in Complex Condition, Ministry of Natural Resources, Changchun 130021, China
[3] CCTEG Chongqing Research Institute, Chongqing 400039, China
[4] Drilling & Production Technology Research Institute, CNPC Chuanqing Drilling Engineering Company Ltd., Guanghan 618300, China
* Correspondence: wangms@jlu.edu.cn; Tel.: +86-04-318-850-2352

Abstract: Down-the-hole (DTH) hammer drilling with reverse circulation is a novel, mobile, high-speed drilling system suitable for the specific requirements of mine rescue. This technology can be applied to shorten the rescue time during mine accidents. The performance of reverse circulation (RC) drilling depends on the structural design of the drill bit. An orthogonal experimental design is executed to investigate the effect of the structural design parameters of the large-diameter drill bit for drilling rescue wells on the cutting carrying capacity and reverse circulation performance. This study employs computational fluid dynamics (CFD) software to solve the Navier–Stokes equation for three-dimensional steady flow and calculate the flow field around the drill bit to evaluate the RC efficiency. Six key geometric parameters were proven to have a direct influence on the RC performance, including the diameter of suction nozzles D_n, the length of nozzles L, the quantity of nozzles N, the diameter of the pilot hole D_g, the inclination angle of nozzles θ_s, and the deflection angle of nozzles θ_d. The CFD simulation experiments were implemented according to the orthogonal array L18(3^7) and were analyzed using the range, variance, and regression analysis. A mathematical model was developed for the RC efficiency to understand the effect of the factors. The results show that the diameter of suction nozzles D_n has an essential effect on the RC performance of the drill bit. An ideal combination is D_n = 20 mm, L = 50 mm, N = 3, D_g = 50 mm, and $\theta_s = 35°$, $\theta_d = 10°$, which was obtained through variance analysis and validated via CFD simulation for higher efficiency. To verify its real performance, a large-diameter RC drill bit with a diameter of 1.2 m was manufactured and tested in the field. The result demonstrated that the drill bit had excellent cutting transport and reverse circulation performance.

Keywords: percussive-rotary drilling; RC drill bit; rescue well drill; orthogonal experimental method; CFD simulation; mine disaster

Citation: Bo, K.; Ji, F.; Zhao, Z.; Fan, L.; Wang, M. Optimum Design of Large-Diameter Reverse Circulation Drill Bit for Drilling Rescue Wells Using Orthogonal Experimental Method and CFD Simulation. *Energies* **2023**, *16*, 3913. https://doi.org/10.3390/en16093913

Academic Editor: Hossein Hamidi

Received: 15 February 2023
Revised: 1 May 2023
Accepted: 2 May 2023
Published: 5 May 2023

1. Introduction

Recently, the demand for mineral resources has increased along with the continual progress in science and technology. The depth of coal mines and metalliferous mines is gradually increasing, which is prone to roof collapse, water seepage, gas leaks, and other accidents. These accidents threaten the health and safety of subterranean miners [1,2]. Underground mining is associated with apparent risks, which may lead to mass-casualty accidents [3]. Some of the most unfortunate previous accidents were the Quecreek mine disaster in the U.S. in 2002, the Chile mine disaster in 2010, and the Pingyi mine disaster in China in 2016 [4–6]. In the above disasters, wellbore drilling is one of the most important means of finding trapped miners, transporting sustenance, and rescuing survivors. Due to

the extremely complex and unstable lithology of the mining area, all rescue operations take a long time, directly affecting the safety and lives of the trapped miners [7].

The emergency rescue must be carried out after a mine accident, but poor rescue results and low efficiency can lead to the deaths of trapped miners [8]. Compared with the conventional mud drilling method, pneumatic DTH hammer drilling, as a percussive-rotary drilling technology, has a higher rate of penetration (ROP) and plays an essential role in mine emergency rescue [9,10]. Furthermore, as an underbalanced drilling technology, the DTH hammer can eliminate formation damage and ensure wellbore stability [11]. There are two types of DTH hammers, direct circulation (DC) and reverse circulation (RC), both of which are equipped with percussive-rotary drilling technology. Due to the relatively large diameter of the rescue well, it is difficult to discharge cutting from the hole bottom to the ground surface using DC drilling [12]. DTH hammer RC drilling is an innovative percussive-rotary drilling technology driven by compressed air and is a potentially effective technology for large-diameter wells [13]. It is a fast and cost-effective way to reduce the air injection rate by at least 70% and improve hole cleaning efficiency [14]. In air RC drilling, compressed air enters the annulus of the dual-wall drill pipe through a dual-wall swivel. The exhaust air then carries the cutting out of the borehole through the center passage rather than the annulus [15]. As shown in Figure 1, the cross-sectional area of the center passage (b) is less than the annular area (a). It is easier to reach the minimum velocity of 15.24 m/s for cutting transport while drilling large-diameter wells.

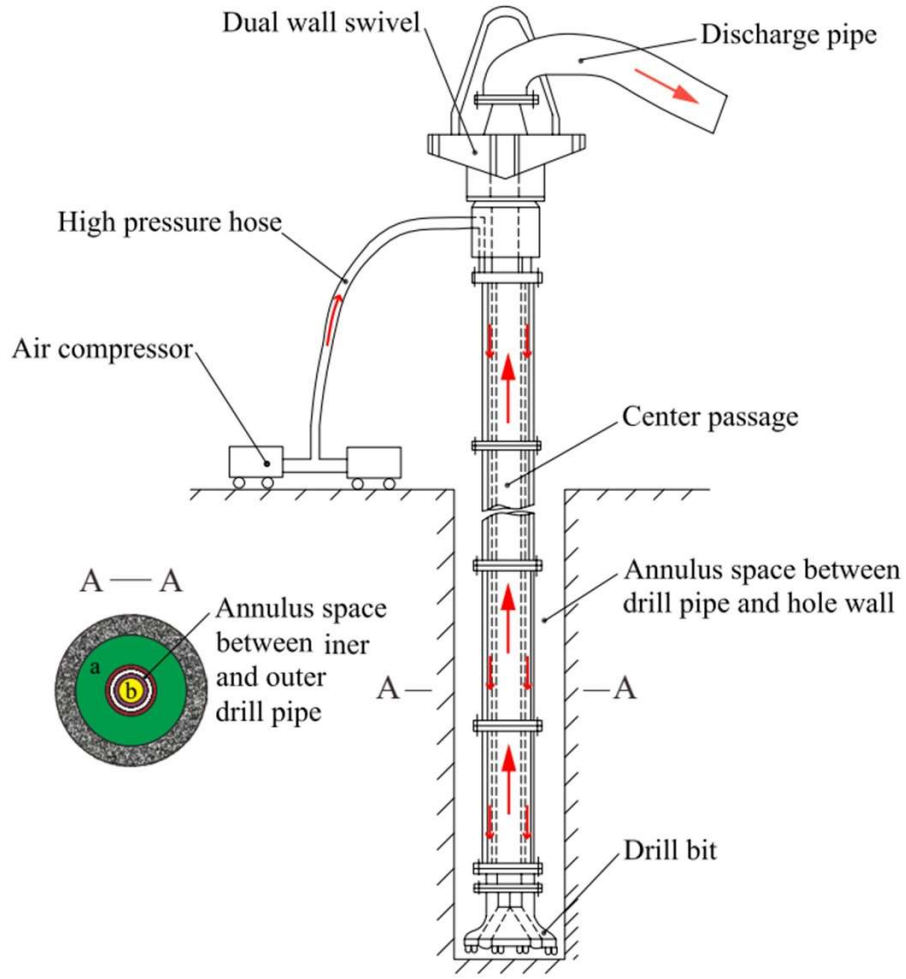

Figure 1. Schematic of large-diameter pneumatic DTH hammer reverse circulation drilling system.

The percussive rotary drilling technology with large-diameter RC pneumatic DTH hammer improves the penetration rate and reduces the energy consumption in drilling

rescue, making rapid rescue feasible. Previous studies show that the RC drill bit is the key component to forming air reverse circulation. Most previous work on RC drilling focused on the structural design of drill bits that control cutting transport at the bottom hole [14–17]. The range of diameters of these RC drill bits studied in previous work was from 80 to 600 mm. However, the existing diameter of the drill bits is still too small for rescue well drilling. It is urgent to develop a large-diameter (>800 mm) RC drill bit for emergency rescue. In this paper, a novel large-diameter RC drill bit was designed through an orthogonal design method. Meanwhile, the effect of the structural parameters of the drill bit on cutting transport and reverse circulation performance was also theoretically and experimentally studied. The influence relationship between the parameters was obtained through range analysis.

2. Structure Design of Large-Diameter RC Drill Bit

In the process of drilling, the RC drill bit, designed specifically based on the ejector principle, is the crucial component and determines the formation of reverse circulation [15]. Figure 2 shows the operational principle of a large-diameter RC bit. After powering the piston, the compressor air flows into the space between the drive sub and the shaft and forms high-velocity air jets via the suction nozzles. The air jets can form a negative pressure zone in the central channel and entrain other air around the drill bit. Under the pressure difference between the bottom hole and the central channel, air can carry cutting into the drilling tools' central channel and returns them to the ground. The greater the pressure difference, the more air is sucked from the annulus into the central channel, and the stronger the suction force for cutting transport.

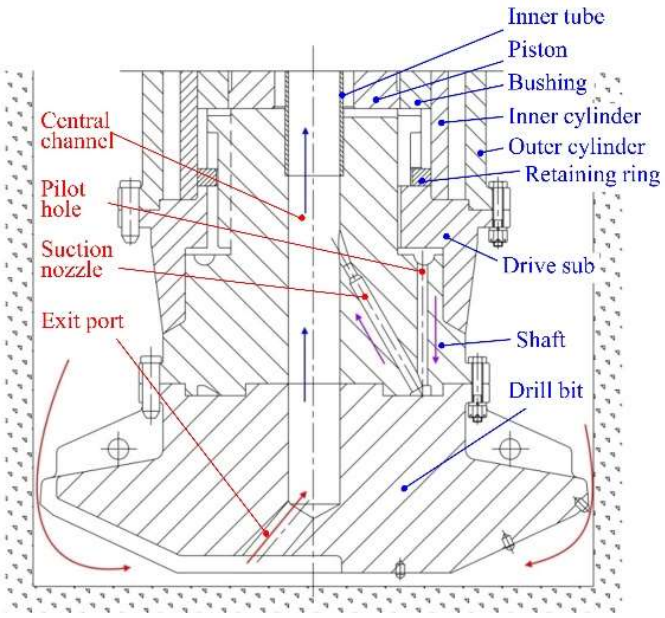

Figure 2. Schematic diagram of pneumatic large-diameter RC bit.

Figure 3 shows seven geometry parameters of the RC drill bit based on the structural characteristics of the large-diameter DTH pneumatic hammer. D_n is the diameter of suction nozzles, N is the number of nozzles, L is the length of nozzles, θ_s is the inclination angle of nozzles, θ_d is the deflection angle of nozzles, D_g is the diameter of the pilot hole, and D_t is the circumferential distribution diameter of the pilot hole.

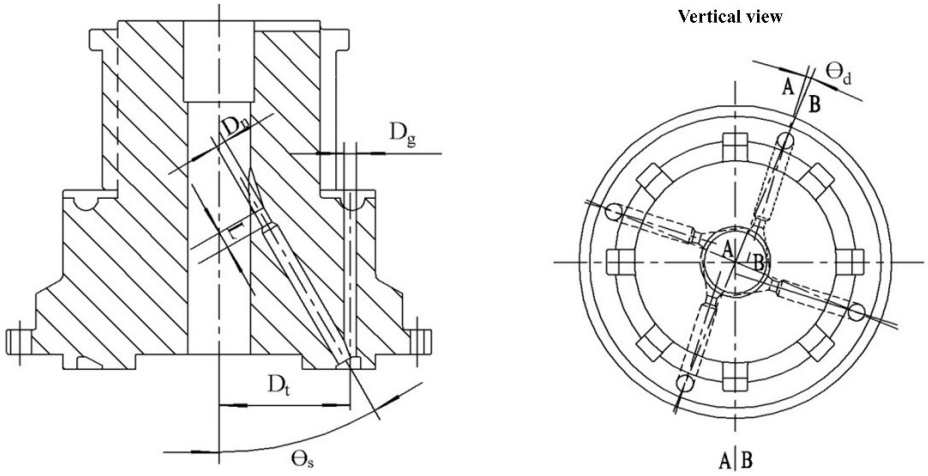

Figure 3. Schematic diagram of structural parameters for RC bit.

3. CFD Simulation Approach

3.1. Computational Domain and Grid

The structural parameter of the RC drill bit with a diameter of 1.2 m was optimized via numerical simulation to investigate the suction capacity. All 18 computational domains were established using Solidworks 2015 and meshed with Hypermesh 10 software. In CFD simulation, grids are the elements of calculation and analysis, and their quality significantly influences calculation accuracy and speed. Poor-quality grids often cause calculation errors much bigger than those generated by the algorithm. To improve computational accuracy and speed, the typical computational domain was divided into five parts: the suction nozzles, the pilot hole, the exit port, the bottom space, and the central channel, as shown in Figure 4. The hexahedral grids were used for the parts that meet the requirements of structural grid topology, while the tetrahedral grid was used for other parts, and the grid density was increased. In this study, structured and unstructured grids were used, with a total number of grids ranging from 0.3 million to 0.4 million. The ratio of the hexagonal grids is 78–92%.

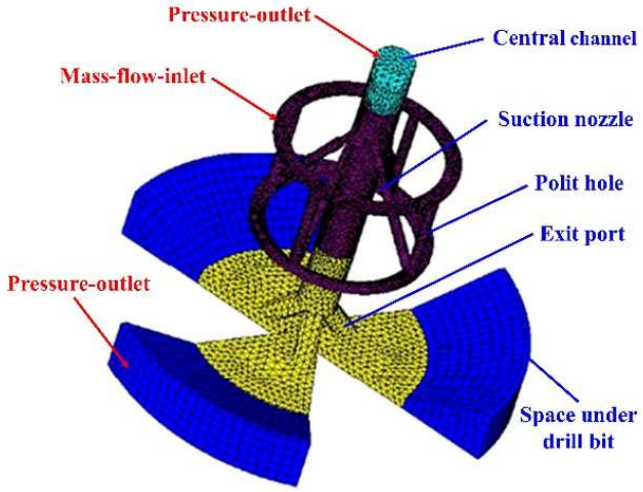

Figure 4. Typical meshed computational domain and the boundary condition types.

3.2. Boundary Conditions

A mass flow inlet boundary condition was used to prescribe mass flow rate at the inlet of the drill bit. Under standard conditions, the rated air flow rate of the DTH hammer to which the drill bit is attached is 50 m^3/min, and the mass flow rate at the inlet of the drill bit is 1.0 kg/s, corresponding to the air volume flow rate of 50 m^3/min, and the initial gauge

pressure was 6×10^5 Pa due to the subsonic inlet velocity. The operating pressure in Fluent 6.3 software was set to 101,325 Pa. The outlets of the central channel and annular space between the drill bit and borehole wall were set to be pressure outlet boundary conditions and were exposed to the atmosphere. Therefore, at these two boundaries, the magnitude of the gauge pressure is set to zero in each computational domain. At rest, in the boundaries of each computational domain, no-slip stationary wall boundary conditions are applied.

The standard wall function method is adopted near the wall. During the analysis process, residual monitoring and the mass flow rate at the inlet and outlet monitoring are set while setting mass flow inlet and pressure outlet boundary conditions and these two monitoring values as the criteria for convergence. The momentum equation, turbulent dissipation rate, and turbulent kinetic energy residuals are 10^{-7}. The continuity equation residuals are 10^{-5}, and the energy equation residuals are 10^{-6}.

3.3. Solver Settings

During the operation of the DTH hammer, the reciprocating piston causes compressed air to flow into the drill bit periodically. Therefore, the airflow is unsteady and compressible. Although air carries cuttings into the central channel in the multiphase flow state, the suction effect of the drill bit mainly depends on the hydrostatic pressure. Using steady-state flow approximation to calculate the flow rate in drill bits is a good compromise solution. A density-based coupled solver (PBCS) solves continuity, momentum, energy, and composition equations in a vector manner and has fast convergence speed and generalization ability. In the solution process of Fluent, the SIMPLEC algorithm is used to discretize the convection term using second-order upwind schemes to improve solution accuracy and convergence speed [18].

Typically, the flow inside the drill bit is turbulent, and a series of turbulence models are available in Fluent. These range from the standard k-ε model to the more complicated Reynolds stress turbulence model. Because the flow inside the central channel of the bit is similar to a multi-nozzle ejector, the realizable k-ε model was chosen. This turbulence model is a more accurate predictor of the divergence ratio of plates and cylindrical jets, providing better separation and recirculation performance.

The second-order upwind discretization was used for convective terms, and the central difference scheme was used for diffusion terms. The coupling between velocity and pressure was dealt with using the Semi-Implicit Method for the Pressure-Linked Equation algorithm. The second-order upwind schemes calculated the turbulent kinetic energy and dissipation rate. Concerning the numerical algorithm, the simulation type was the steady state, and high-resolution discretization was adopted for advection terms, with the first-order upwind schemes for turbulence numeric. To prevent convergence oscillation or divergence during the calculation process and ensure a fast convergence speed, the physical timescale is 10^{-3} s, and the convergence target is 10^{-4}.

3.4. CFD Modeling

The internal airflow is considered to follow the principles of conservation of mass, momentum, and energy. The general governing equation is [19]:

$$\frac{\partial(\rho\phi)}{\partial t} + div(\rho u\phi) = div(\Gamma grad\phi) + S \quad (1)$$

where ρ is density; ϕ is the generic variable; u is the velocity vector; Γ is the generalized diffusion coefficient; S is the generalized source term.

In the realizable k-ε model, the turbulent viscosity is calculated by using an improved method, and, therefore, the realizable k-ε is considered more accurate in predicting the

distribution of the dissipation rate of flat and round jets. The k equation and ε equation are expressed as follows [20,21]:

$$\frac{\partial(\rho k)}{\partial t} + \frac{\partial(\rho k u_j)}{\partial x_j} = \frac{\partial}{\partial x_j}\left[\left(\mu + \frac{\mu_i}{\sigma_k}\right)\frac{\partial k}{\partial x_j}\right] + G_k - \rho\varepsilon \tag{2}$$

$$\frac{\partial(\rho \varepsilon)}{\partial t} + \frac{\partial(\rho \varepsilon u_j)}{\partial x_j} = \frac{\partial}{\partial x_j}\left[\left(\mu + \frac{\mu_i}{\sigma_\varepsilon}\right)\frac{\partial \varepsilon}{\partial x_j}\right] + \rho C_1 E\varepsilon - \rho C_2 \frac{\varepsilon^2}{k + \sqrt{v\varepsilon}} \tag{3}$$

where C_1 is defined as:

$$C_1 = \max\left(\frac{\eta}{\eta + 5}, 0.43\right) \tag{4}$$

$$\eta = E\frac{k}{\varepsilon} = \sqrt{(2E_{ij}E_{ij})}\left(\frac{k}{\varepsilon}\right) \tag{5}$$

$$E_{ij} = \frac{1}{2}\left(\frac{\partial u_i}{\partial x_j} + \frac{\partial u_j}{\partial x_i}\right) \tag{6}$$

where u_i and u_j are the mean components of the velocity; x_j and x_j are the Cartesian coordinates; μ is the dynamic molecular viscosity, v is the kinematic viscosity; μ_i is eddy viscosity; G_k is the generation of turbulence kintic energy due to mean velocity gradients; σ_k and σ_ε are the turbulent Prandtl number for k and ε, respectively; the following standard closure coefficients are: $C_2 = 1.9$, $\sigma_k = 1.0$, and $\sigma_\varepsilon = 1.2$.

4. Orthogonal Experimental Design

The orthogonal method is a unique and robust experimental design and statistical technique used to optimize performance, quality, and cost. It is widely used in engineering analysis to improve performance [22–24]. The orthogonal method is a helpful tool that efficiently improves experimental work by using fewer experiments to identify and optimize parameters in order to achieve desired results. Orthogonal arrays were employed to design numerical experiments with structural parameters influencing reverse circulation performance [25]. Orthogonal experimental design includes the selection of factors, levels, and experimental schemes [26,27]. If we chose three variables for each parameter during the optimal design of structural parameters, the total number of models would be 3^7 (2189). The simulation calculation will become burdensome, and data analysis and revealing laws will be complicated [28]. When the orthogonal array $L_{18}(3^7)$ is used to arrange CFD simulations scientifically, the number of experiments will be significantly reduced, and data statistics will also be simplified, making it easier to find the optimal parameter combination.

4.1. Two-Level Orthogonal Experimental Design

We selected a seven-factorial two-level L_8 (2^7) orthogonal array according to the structural parameters of the RC drill bit shown in Figure 3 and determined the range of parameter changes. Meanwhile, we determined each parameter's primary and secondary order and checked for any interactions between the two parameters. In the process of simulation analysis, the entrained air mass flow rate Q_a at the annulus between the drill bit and borehole was used as the assessment index. When $Q_a > 0$, it indicates that the outer annulus air is being sucked into the central channel, and the value of Q_a represents the drill bit's suction capacity. The larger the value is, the stronger the suction capacity is and the better the reverse circulation efficiency. When $Q_a = 0$, it indicates that the compressed air neither sucks air from the outer annulus nor enters the annulus after passing through the nozzle of the drill bit. When $Q_a < 0$, it indicates that the drill bit cannot suck air from the outer annulus and reverse circulation fails. This situation should be avoided in the design.

Table 1 lists the combinations of design parameters used in the orthogonal array for the eight repetitions of the RC drill bit. The effect of each parameter on the drill bit's RC

efficiency was evaluated using variance analysis, and the magnitude of the range R reflects the effect of various factors on the experimental evaluation index. Since the range R of D_t is tiny, it can be regarded as a minor influence that can be ignored in the high-level orthogonal experimental design to reduce the amount of calculation.

Table 1. L_8 (2^7) orthogonal array of design combinations and range analysis.

No.	Design Factors							Q_a
	D_n/mm	L/mm	N	D_g/mm	θ_s/°	θ_d/°	D_t/mm	kg/s
1	25	40	4	40	30	5	630	1.9206
2	25	40	4	45	35	10	640	2.5082
3	25	50	5	40	30	10	640	1.5829
4	25	50	5	45	35	5	630	1.8185
5	30	40	5	40	35	5	640	0.9605
6	30	40	5	45	30	10	630	0.9981
7	30	50	4	40	35	10	630	1.9246
8	30	50	4	45	30	5	640	1.6823
K_1	7.8302	6.3874	8.0357	6.3886	6.1839	6.3819	6.6618	
K_2	5.5655	7.0083	5.3600	7.0071	7.2118	7.0138	6.7339	
k_1	1.9576	1.5969	2.0089	1.5972	1.5460	1.5955	1.6655	
k_2	1.3914	1.7521	1.3400	1.7518	1.8030	1.7535	1.6835	
R	0.5662	0.1552	0.6689	0.1546	0.2570	0.1580	0.0180	
order	2	6	1	5	3	4	7	

Further, 21 combination models of pairwise interactions between seven parameters were studied computationally using Fluent to exclude the influence of interaction terms on orthogonal experimental results. All figures similar to Figure 5 were obtained. Considering the influence of experimental errors, if two straight lines are approximately parallel, it can be confirmed that there is no interaction between the two factors. It is judged that there is no interaction between the parameters. We ignored high-level interaction items (more than two factors) and classified their influence on the experimental result as error items.

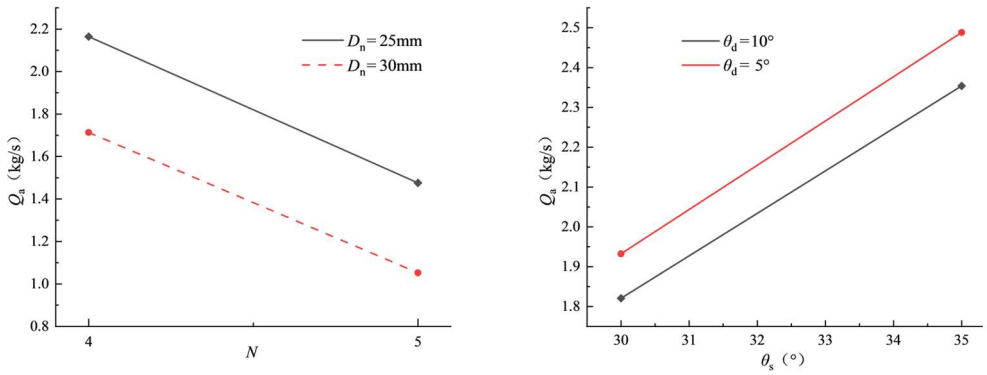

(**a**) (**b**)

Figure 5. Interaction decision diagram. (**a**) Interaction between diameter and number of nozzles; (**b**) interaction between inclination and deflection angle of the nozzle.

4.2. Three-Level Orthogonal Experimental Design

According to previous theoretical analysis and experimental research, six design factors (A, B, C, D, E, F) were chosen as the core design parameters for optimizing the RC efficiency of the drill bit. A is the diameter of suction nozzles D_n, B is the number of nozzles N, C is the length of nozzles L, D is the diameter of pilot hole D_g, E is the inclination angle of nozzles θ_s, and F is the deflection angle of nozzles θ_d. Table 2 lists each design parameter's constraints and evaluates the primary and secondary parameter order using

seven-factorial three-level L_{18} (3^7) orthogonal arrays. The constraints selected for this study are parameters that do not affect the RC drill bit's machinability, connectivity, and durability. Three levels were assigned to each design factor used in the orthogonal method (in Table 3) to approximate the experimental conditions of practical optimization.

Table 2. Constraints on design parameters.

Design Factors	Lower Limit	Parameters	Upper Limit
A	15≤	Diameter of suction nozzles D_n	≤35
B	20≤	Length of nozzles L	≤70
C	2≤	Number of nozzles N	≤6
D	35≤	Diameter of pilot hole D_g	≤55
E	20≤	Inclination angle of nozzles θ_s	≤40
F	0≤	Deflection angle of nozzles θ_d	≤20

Table 3. Orthogonal experimental factors.

Factors	Factors Notation	A D_n/mm	B L/mm	C N	D D_g/mm	E θ_s/°	F θ_d/°
Levels	1	20	30	3	40	25	0
	2	25	40	4	45	30	5
	3	30	50	5	50	35	10
interval		5	10	1	5	5	5

5. Result and Discussion

5.1. Orthogonal Experiment Results

Table 4 presents the L18 (3^7) orthogonal arrays of the level combinations of design factors in the orthogonal experimental method. On this basis, we conducted CFD analysis on 18 models of optimized drill bits and obtained predicted reverse circulation efficiency values under a specific mass flow rate. These 18 experimental models were used to test all of the pairwise combinations of the independent variables. It demonstrates significant savings in test workload and expense compared to the all-combination approach. Due to the orthogonal feature, the importance order of each factor could be achieved through variance analysis [29]. In addition, numerical simulation experiments can reduce drill bit manufacturing costs and shorten design cycles.

Judging by the orthogonal method, the sensitivity of the parameters of the RC drill bit can be obtained through range analysis based on the simulation results in Table 4. The extreme difference of each parameter can be calculated as follows:

$$K_i = \sum_{j=1}^{6} Q_{ij} \; ; \; k_i = \frac{K_i}{6} \; (i = 1,2,3; j = 1,2,3,4,5,6) \tag{7}$$

$$R = \max(k_i) - \min(k_i) \tag{8}$$

where Q_{ij} is the RC efficiency of the drill bit, K_i is the sum of the RC efficiency for a specific parameter whose level index is i, k_i is the average RC efficiency for a certain parameter whose level index is i, and R is the extreme difference of the parameter. Figure 6 depicts the effect of each design parameter on RC efficiency, as revealed by the screening.

Table 4. L_{18} (3^7) orthogonal experimental design and CFD simulation results.

No.	A D_n/mm	B L/mm	C N	D D_g/mm	E θ_s/°	F θ_d/°	G *null*	Q_a kg/s
1	1	1	1	1	1	1	1	2.074
2	1	2	2	2	2	2	2	2.214
3	1	3	3	3	3	3	3	2.716
4	2	1	1	2	2	3	3	2.859
5	2	2	2	3	3	1	1	2.136
6	2	3	3	1	1	2	2	1.353
7	3	1	2	1	3	2	3	1.560
8	3	2	3	2	1	3	1	1.331
9	3	3	1	3	2	1	2	2.010
10	1	1	3	3	2	2	1	2.255
11	1	2	1	1	3	3	2	3.481
12	1	3	2	2	1	1	3	2.055
13	2	1	2	3	1	3	2	2.168
14	2	2	3	1	2	1	3	1.397
15	2	3	1	2	3	2	1	2.737
16	3	1	3	2	3	1	2	1.198
17	3	2	1	3	1	2	3	1.709
18	3	3	2	1	2	3	1	1.871

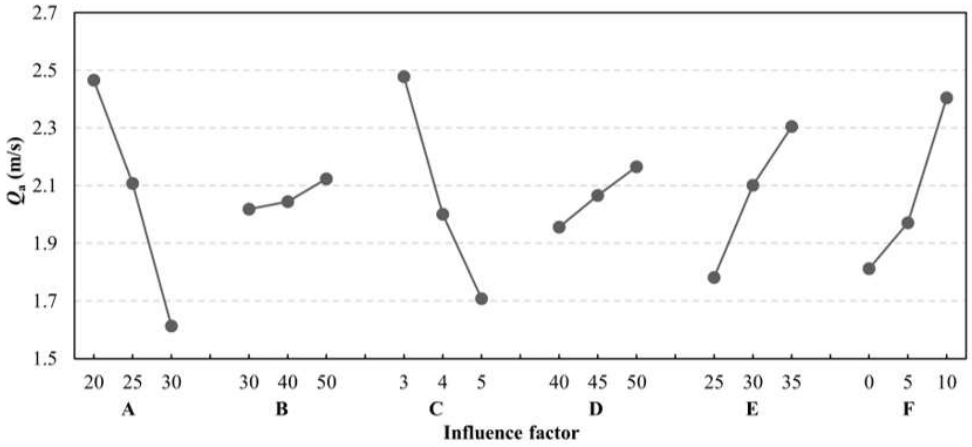

Figure 6. Main effect plot of design parameter for reverse circulation efficiency.

The larger the extreme difference, the higher the corresponding parameter sensitivity. In other words, the effect of each parameter on RC efficiency is more significant when its range R is larger. The analysis results for RC efficiency are shown in Table 5 and Figure 6. We find that the factors influencing RC efficiency decrease in the following order: $A > C > F > E > D > B$. The diameter of suction nozzles D_n is the most important determinant of RC efficiency. When factor A employs a value of 20 mm, the RC drill bit has the best RC efficiency. Factor B has a lower significance on RC efficiency compared to other factors. The reason may be that the air injection rate determines the suction capacity. Their changing trends have an obvious peak value for all six factors. Each parameter has an optimal value or level for better efficiency. Consequently, the best optimal combination for better efficiency is A_1, B_3, C_1, D_3, E_3, and F_3, namely: D_n = 20 mm, L = 50 mm, N = 3, D_g = 50 mm, θ_s = 35°, and θ_d = 10°. Although it is not in the orthogonal array, it indicates that the optimization results reflect the tests conducted and the comprehensive test information. We established a model based on the optimal combination of parameters and conducted CFD simulation. The assessment index Q_a = 3.575 kg/s and has the best efficiency. The simulation results also validated the orthogonal experimental method's balanced dispersion and comprehensive comparability.

Table 5. Results of the range analysis for the orthogonal experimental method.

Factor	D_n/mm	L/mm	N	D_g/mm	θ_s/°	θ_d/°	*null*
K_1	14.795	12.114	14.870	11.736	10.690	10.870	12.404
K_2	12.650	12.268	12.004	12.394	12.606	11.828	12.424
K_3	9.679	12.742	10.250	12.994	13.828	14.426	12.296
k_1	2.4658	2.0190	2.4783	1.9560	1.7817	1.8117	2.0673
k_2	2.1083	2.0447	2.0007	2.0657	2.1010	1.9713	2.0707
k_3	1.6132	2.1237	1.7083	2.1657	2.3047	2.4043	2.0493
R	0.8527	0.1047	0.7700	0.2097	0.5230	0.5927	0.0213
sorting	1	6	2	5	4	3	7
optimal level	1	3	1	3	3	3	2
optimal design	D_n(20)	L(50)	N(3)	D_g(50)	θ_s(35)	θ_d(10)	

5.2. Variance and Regressive Analysis

Variance analysis is adopted to analyze the orthogonal experimental results and determine the priority levels of factors. The total sum of deviation squares (SS_T) and the sum of the deviation squares caused by j row (SS_j) are calculated using Equations (9) and (10) [30].

$$SS_T = \sum_{i=1}^{n} (y_i - \overline{y})^2 = \sum_{i=1}^{n} {y_i}^2 - n\overline{y}^2 \tag{9}$$

$$SS_j = \frac{r}{n} \sum_{i=1}^{n} {K_{ij}}^2 - \frac{1}{n} \left| \sum_{i=1}^{n} y_i \right|^2 \tag{10}$$

The variance for each factor is calculated via Equation (11)

$$MS_j = SS_j / df_j \tag{11}$$

where i is different experimental number, j is the different factors, y_i is the experimental result at number i, $\overline{y}$ is the average value of experimental results, n is the total number of experiments, K_{ij} is the experimental result of factor j at level i, r is experimental number at each level, and df_j is the freedom defined at level number minus one.

The variance ratio is calculated using Equation (12), where the denominator is the error variance.

$$F_j = \frac{SS_j / df_j}{SS_e / df_e} = \frac{MS_j}{MS_e} \sim F(df_j, df_e) \tag{12}$$

In optimizing the design of the drill bit, special attention should be paid to the parameters of significant influencing factors [31,32]. Table 6 shows the calculated results from the above equations and verifies the signature of each factor according to the F-distribution law $F_a(df_j, df_e)$, where df_j and df_e are the freedoms of factors and error terms in the variance ratio. It can be seen that A (diameter of nozzles), C (length of nozzles), E (inclination angle of nozzles), and F (deflection angle of nozzles) have a significant influence on RC efficiency. Furthermore, the results derived from variance analysis agree with those from the previous range analysis.

The correlations between Q_a and the key factors were studied via regression analysis based on simulation data. The optimized regression equation includes all significant factors to index Q_a. The probable equation can be assumed to be nonlinear. To improve calculation efficiency, the regression equation did not consider the interaction of factors and only regressed the linear and quadratic terms of each factor.

$$\begin{aligned} Q_a = a + b_1 D_n + b_2 {D_n}^2 + b_3 L + b_4 L^2 + b_5 N + b_6 N^2 + b_7 D_g + b_8 {D_g}^2 + b_9 \theta_s \\ + b_{10} {\theta_s}^2 + b_{11} \theta_d + b_{12} {\theta_d}^2 \end{aligned} \tag{13}$$

Table 7 presents the calculated results of the coefficients for each factor, and a nonlinear mathematical model can be written as follows.

$$Q_a = 0.485 + 0.052 * D_n - 0.005 * {D_n}^2 - 0.016 * L - 1.126 * N + 0.093 * N^2 + 0.038 * D_g + 0.191\theta_s - 0.002 * {\theta_s}^2 + 0.005 * \theta_d + 0.005{\theta_d}^2 \quad (14)$$

The *F* test shows that the significance level of the final mathematical model is 0.001, indicating that the reliability of the mathematical model is 99.9%.

Table 6. Significance of each factor via variance analysis **.

Variance Factors	SS_j	df_j	MS_j	*F* Value	Significance
A(D_n)	2.200	2	1.100	51.402	**
B(L)	0.036	2	0.018	0.841	
C(N)	1.813	2	0.907	42.360	**
D(D_g)	0.132	2	0.066	3.084	
E(θ_s)	0.834	2	0.417	19.486	**
F(θ_d)	1.129	2	0.565	26.379	**
e$^{\triangle}$	0.107	5	0.021		
F			$F_{0.05}(2,5) = 5.79$		$F_{0.01}(2,5) = 13.27$

Table 7. Coefficients of the variables in the regression equation.

	Constant	D_n	${D_n}^2$	L	L^2	N	N^2	D_g	${D_g}^2$	θ_s	${\theta_s}^2$	θ_d	${\theta_d}^2$
Coefficients	0.485	0.052	−0.003	−0.016	0.000	−1.126	0.093	0.038	0.000	0.191	−0.002	0.005	0.005
Std. error	6.892	0.147	0.003	0.059	0.001	0.589	0.073	0.264	0.003	0.176	0.003	0.031	0.003
t Stat	0.070	0.356	−0.938	−0.274	0.363	−1.914	1.263	0.145	−0.066	1.084	−0.788	0.151	1.863
p-value	0.947	0.736	0.391	0.795	0.731	0.114	0.262	0.890	0.950	0.328	0.466	0.886	0.122

5.3. Influence of Parameter Variation on RC Efficiency

On the premise that the airflow rate is invariable, the regression equation obtained from regression analysis and simulation of the Q_a value from the orthogonal array summarizes the influence of significant parameter variation on the RC efficiency.

5.3.1. Influence of Nozzle Diameter D_n Variation on Annulus Mass Flow Q_a

Figure 7 shows the influence law of D_n variation on annular mass flow Q_a when L and D_g are changed. The curves show that when D_g and D_n remain constant and L changes, the amplitude of Q_a is very small. When L and D_g remain constant and D_n increases from 15 mm to 35 mm, the Q_a value increases first and then decreases, reaching its maximum when D_n = 20 mm.

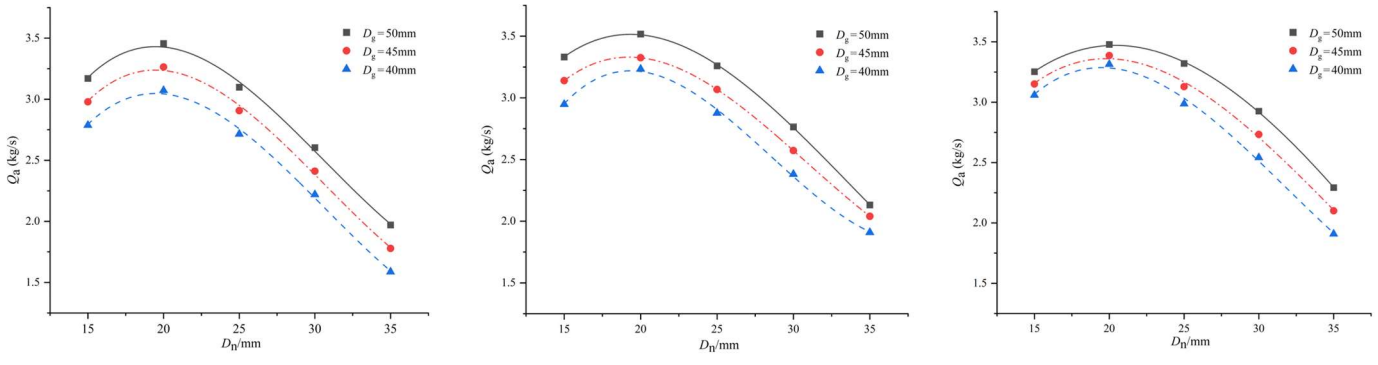

Figure 7. Effect of D_n on Q_a at different D_g. (**a**) L = 50 mm; (**b**) L = 40 mm; (**c**) L = 30 mm.

When the compressed air ejects through the nozzle at high velocity, it will entrain the low-velocity fluid, called the Venturi effect. It generates a negative pressure zone at the bottom of the drill bit, leading to the air in the annulus being suctioned into the central channel. With a pressure gradient, the air carries the cutting back to the ground through the central channel of drill tools. When the value of D_n is too small, the local pressure loss of the nozzle and backpressure under the piston increase, and the energy of compressed air cannot convert into the impact energy of the piston, resulting in energy wastage. When the value of D_n is too large, the air velocity decreases, and the suction force weakens. Therefore, the optimal value of D_n is about 20 mm.

5.3.2. Influence of Nozzle Quantity N Variation on Annulus Mass Flow Q_a

Figure 8 shows the influence law of N variation on annular mass flow Q_a when D_g and D_n are changed. The curves show that when N and D_n remain constant and D_g changes, the amplitude of Q_a is very small. When D_g and D_n remain constant and L increases from 2 to 6, the Q_a value increases first and then decreases, reaching its maximum when N = 3.

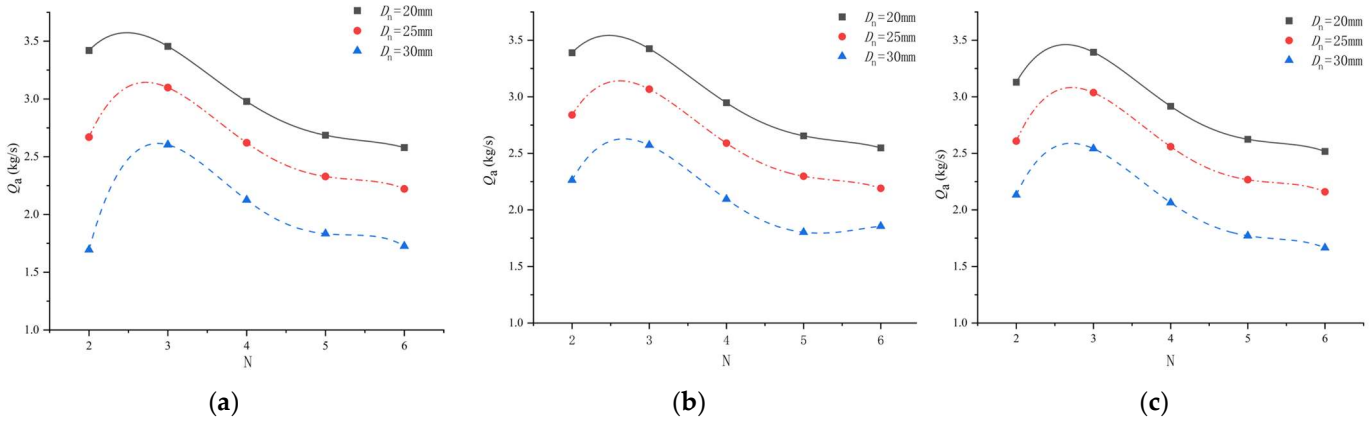

Figure 8. Effect of N on Q_a at different D_g. (**a**) D_g = 50 mm; (**b**) D_g = 45 mm; (**c**) D_g = 40 mm.

When D_n is constant and N increases, the cross-sectional area of the nozzles increases, and suction ability weakens. Moreover, there will be interference between the ejected air, which is not conducive to forming a negative pressure zone on the hole bottom. In addition, when N is small, the local pressure loss through the nozzle increases, resulting in energy loss and a weakening of suction force.

5.3.3. Influence of Nozzle Deflection Angle θ_s Variation on Annulus Mass Flow Q_a

Figure 9 shows the influence law of θ_s variation on annulus mass flow Q_a when D_n and θ_d remain constant. The curves show that when θ_s and θ_d remain constant and D_n changes, the amplitude of Q_a is large. When θ_d and D_n remain constant and θ_s increases from 20° to 40°, the Q_a value increases first and then decreases. Regardless of the combination of θ_d and D_n, the Q_a reaches the maximum when θ_s = 35°.

When the inclination angle of the nozzle is too small, the distance of fluid flow will be long, and the frictional loss will increase, thus reducing the entrainment capacity of the high-velocity air jet. When the inclination angle is too large, the high-velocity air jet directly hits the inner wall of the central channel, resulting in diffuse reflection and turbulence of the fluid. This is unfavorable for the air jet to suck air from the outer annulus into the central channel. In the drill bit design process, the nozzle's inclination angle should be as close as possible to 35°.

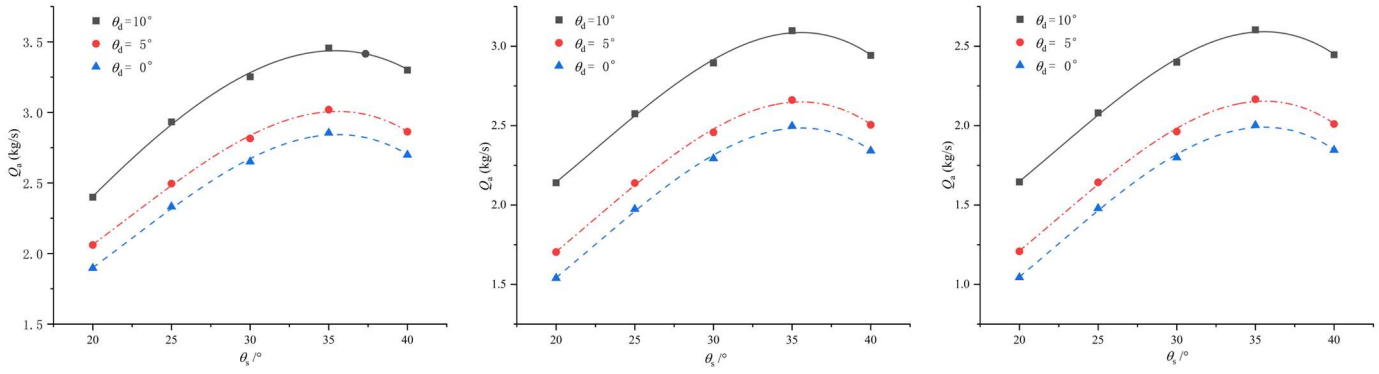

Figure 9. Effect of θ_s on Q_a at different θ_d. (**a**) D_n = 20 mm; (**b**) D_n = 30 mm; (**c**) D_n = 40 mm.

5.3.4. Influence of Nozzle Inclination Angle θ_d Variation on Annulus Mass Flow Q_a

Figure 10 shows the influence law of θ_d variation on annulus mass flow Q_a when D_n and θ_s remain constant. The curves show that when θ_s and θ_d remain constant and D_n changes, the amplitude of Q_a is large. When θ_s and D_n remain constant and θ_d increases from 0° to 20°, the Q_a value increases first and then decreases. Regardless of the combination of θ_s and D_n, the Q_a reaches the maximum when θ_d = 10°.

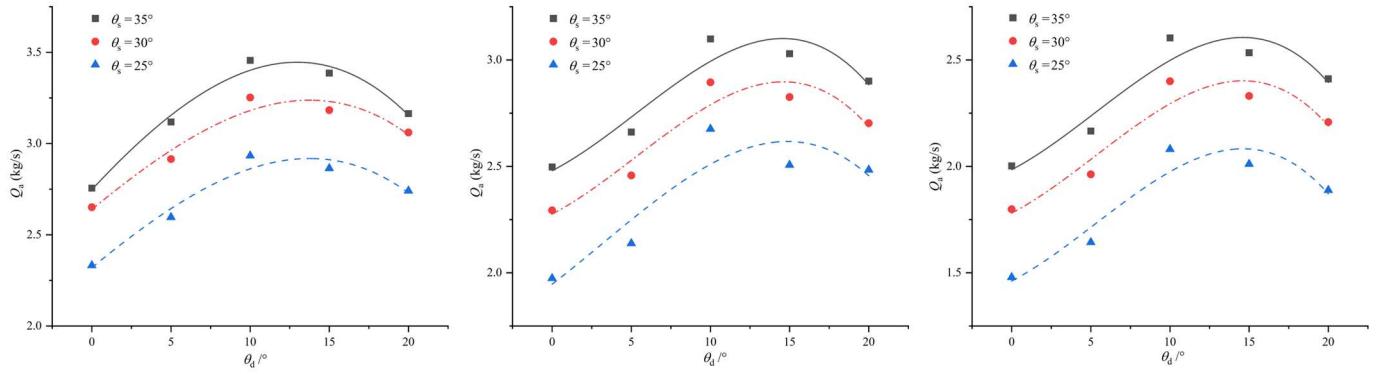

Figure 10. Effect of θ_d on Q_a at different θ_s. (**a**) D_n = 20 mm; (**b**) D_n = 30 mm; (**c**) D_n = 40 mm.

When the nozzle has a certain deflection angle, the compressed air will spiral up along the inner wall of the central channel after being ejected at high velocity through the nozzle. This increases the suction effect of the air jet on the outer annulus air. When the deflection angle increases to a certain angle, the high-velocity airflow from the nozzle will collide with the inner wall of the central channel, causing turbulence. This turbulence is not conducive to entraining air in the outer annulus. In the drill bit design process, the nozzle's deflection angle should be as close as possible to 10°.

In the present study, the air jet's flow characteristics and pressure distribution directly affect the suction effect. The suction capacity of the nozzles determines the reverse circulation performance. The greater the suction capacity of the drill bit, the better the RC efficiency. Due to the mutual interference between multiple airflows, the reasonable selection of the structure parameters of nozzles, including diameter, number, and angles, is advantageous in improving suction capacity. The amount of parameter combinations is large, and it is challenging to find the law. The orthogonal experimental design becomes a practical tool for finding the optimal combination and enhancing the suction capacity of the drill bit.

As shown in Figure 11, the rapid rescue drilling technology with the pneumatic DTH hammer was conducted with the RC drill bit based on this study. The DTH hammer

matched with the rotary drill rig was utilized for a field test, and two compressors provided compressed air. Drill cutting returned to the ground is primarily middle-sized particles. Moreover, no cutting sinking slag was found in the borehole during the flushing process, and the cutting can return to the ground continuously. It can conclude that the large-diameter RC drill bit was in good working condition and exhibited outstanding performance in rapid reuse well drilling.

Figure 11. Photographic image of large-diameter DTH hammer and RC drill bit.

6. Conclusions

In this paper, the optimization of structural parameters on the RC efficiency of the drill bit by using the orthogonal experimental method and CFD simulation was performed. The main results were as follows:

(1) The simulation result analysis shows that CFD simulation combined with the orthogonal method is of great significance in studying RC efficiency. Using the above two research methods, the optimization design of the large-diameter RC drill bit provides a low-cost and efficient way to predict RC efficiency

(2) Range analysis shows the primary and secondary factors and optimal levels in six critical structural parameters. Then, a combination of parameters is obtained using optimal theory. The primary and secondary sequence of design parameters is the diameter of nozzles (D_n), the number of nozzles (N), the deflection angle of nozzles (θ_d), the inclination angle of nozzles (θ_s), the diameter of pilot hole (D_g), and the length of nozzles (L).

(3) When the air volume of the DTH hammer is 50 m^3/min and the diameter of the drill bit is 1.2 m, a configuration of parameters with D_n = 20 mm, N = 3, L = 50 mm, θ_s = 50°, and θ_d = 10°, D_g = 50 mm are the ideal parameter combinations. In this condition,

Q_a = 3.575 kg/s and is more than any parameter combination in the orthogonal array L_{18} (3^7).

(4) The successful usage of the DTH hammer drilling method with an RC drill bit also shows good application prospects for drilling hard rock in large-diameter rescue wells. The application is feasible because the static pressure in the central channel is considerably less than that in the annulus, thereby allowing for smooth cutting transport by applying a low input volume flow rate and saving equipment and fuel consumption. Thus, further investigation into the drill bit and technical parameters using reverse circulation DTH hammer is recommended.

Author Contributions: K.B.: conceptualization, methodology, original draft, supervision and funding acquisition; F.J.: methodology, validation, formal analysis; Z.Z.: methodology, validation, CFD simulation; L.F.: formal analysis, visualization; M.W.: methodology, formal analysis, supervision. All authors have read and agreed to the published version of the manuscript.

Funding: This research was funded by the Natural Science Foundation of Jilin Province, China, grant Number 20210101102JC.

Data Availability Statement: Not applicable.

Conflicts of Interest: The authors declare no conflict of interest.

References

1. Reddy, A.H.; Kalyan, B.; Murthy, C.S.N. Mine Rescue Robot System: A Review. *Procedia Earth Planet. Sci.* **2015**, *11*, 457–462. [CrossRef]
2. Murphy, R.; Kravitz, J.; Stover, S. Mobile robots in mine rescue and recovery. *IEEE Robot Autom. Mag.* **2009**, *16*, 91–103. [CrossRef]
3. Aléx, J.; Lundin, H.; Joansson, C.; Saveman, B. Preparedness of Swedish EMS Personnel for Major Incidents in Underground Mines. *J. Health Sci.* **2017**, *5*, 239–243.
4. Tao, Y.; DU Bing-jian, K. Construction Technology of Large Diameter Rescue Borehole in Pingyi Gypsum Mine Disaster of Shandong. *Explor. Eng. (Rock Soil Drill. Tunn.)* **2017**, *44*, 19–23. (In Chinese)
5. Junginger, S. The Chile Miner Rescue: A Human-centred Design Reflection. *Des. J.* **2012**, *15*, 169–183. [CrossRef]
6. Gang, Z.; Hong-bin, Q.; Gao-wei, J.; De-po, L. Research on equipments arrangement in rescuing operations of coal mine inundation. *Procedia Earth Planet. Sci.* **2009**, *1*, 269–274. [CrossRef]
7. He, J.; Zhao, Z.; Yin, Q.; Luo, Y.; Gan, X. Design and optimisation on rapid rescue well-drilling technology with large-diameter pneumatic hammers. *Int. J. Min. Reclam. Environ.* **2020**, *34*, 19–33. [CrossRef]
8. Zheng, X.; Wang, H.; Guo, J.; Zhang, D. Method for multi-information drilling detection after mining disasters. *Comput. Electr. Eng.* **2020**, *86*, 106726. [CrossRef]
9. Kivade, S.B.; Murthy, C.S.N.; Vardhan, H. ANN Models for Prediction of Sound and Penetration Rate in Percussive Drilling. *J. Inst. Eng.* **2015**, *96*, 93–103. [CrossRef]
10. Bo, K.; Sun, S.; Hu, Y.; Wang, M.; Ling, Z.; Zhou, L. Design Optimization and Performance Analysis of the Pneumatic DTH Hammer with Self-Propelled Round Bit. *Shock Vib.* **2021**, *2021*, 6653390. [CrossRef]
11. Arabjamaloei, R.; Edalatkhah, S.; Jamshidi, E. A New Approach to Well Trajectory Optimization Based on Rate of Penetration and Wellbore Stability. *Pet. Sci. Technol.* **2011**, *29*, 588–600. [CrossRef]
12. Cao, P.; Chen, Y.; Liu, M.; Chen, B.; Wang, J. Analytical and experimental study of a reverse circulation drill bit with an annular slit. *Adv. Mech. Eng.* **2016**, *8*, 1687814016669471. [CrossRef]
13. Cao, P.; Cui, G.; Qi, B.; Yao, S.; Zheng, Z.; Bo, K. Investigation on the cuttings carrying capacity of a novel retractable drill bit used in casing while drilling with air reverse circulation. *J. Pet. Sci. Eng.* **2022**, *219*, 111079. [CrossRef]
14. Yang, X.; Guo, B.; Timiyan, T.A. Analytical and Numerical Simulation of Asymmetric Converging Flow of Gas Under Drill Bits in Reverse Circulation Gas Drilling. *J. Energy Resour. Technol.* **2022**, *144*, 043201. [CrossRef]
15. Zhang, X.; Luo, Y.; Gan, X.; Yin, K. Design and numerical analysis of a large-diameter air reverse circulation drill bit for reverse circulation down-the-hole air hammer drilling. *Energy Sci. Eng.* **2019**, *7*, 921–929. [CrossRef]
16. Cao, P.; Chen, Y.; Liu, M.; Chen, B. Optimal Design of Novel Drill Bit to Control Dust in Down-the-Hole Hammer Reverse Circulation Drilling. *Arab. J. Sci. Eng.* **2018**, *43*, 1313–1324. [CrossRef]
17. Luo, Y.; Shi, E.; Feng, Y.; Guo, B.; Zhang, L. Finite Element Investigation of Flow Field Below Asymmetric Drill Bits for Reverse Circulation in Drilling Tight Oil and Gas Reservoirs. *Comput. Model. Eng. Sci.* **2019**, *121*, 105–122. [CrossRef]
18. Song, X.; Lv, Z.; Li, G.; Hu, X.; Shi, Y. Numerical analysis of characteristics of multi-orifice nozzle hydrothermal jet impact flow field and heat transfer. *J. Nat. Gas Sci. Eng.* **2016**, *35*, 79–88. [CrossRef]
19. Zhu, J.; Huang, Z.; Ma, Y.; Xie, D.; Yang, X.; Zhou, C. Hydraulic structure design and downhole flow field optimization of geophysical drill bits in a limestone stratum. *Sci. Prog.* **2020**, *103*, 0036850420931257. [CrossRef]

20. El-Amin, M.F.; Sun, S.; Heidemann, W.; Müller-Steinhagen, H. Analysis of a turbulent Buoyant confined jet modeled using realizable k–ε model. *Heat Mass. Transf.* **2010**, *46*, 943–960. [CrossRef]
21. Shaheed, R.A.R.U. A comparison of standard k–ε and realizable k–ε turbulence models in curved and confluent channels. *Environ. Fluid Mech.* **2019**, *19*, 543–568. [CrossRef]
22. Xiang, H.; Lei, B.; Li, Z.; Zhao, K.; Lv, Q.; Zhang, Q.; Geng, Y. Analysis of Parameter Sensitivity of Induction Coil Launcher Based on Orthogonal Experimental Method. *IEEE Trans. Plasma Sci.* **2015**, *43*, 1198–1202. [CrossRef]
23. Gaitonde, V.N.; Achyutha, B.T.; Siddeswarappa, B. Burr size minimization in drilling using Taguchi technique. *Indian J. Eng. Mater. S* **2005**, *12*, 91–96.
24. Cakiroglu, R.; Acir, A. Optimization of cutting parameters on drill bit temperature in drilling by Taguchi method. *Measurement* **2013**, *46*, 3525–3531. [CrossRef]
25. Luo, Y.; Peng, J.; Li, L.; He, J.; Gan, X.; Yin, K.; Zhao, Z. Development of a specially designed drill bit for down-the-hole air hammer to reduce dust production in the drilling process. *J. Clean Prod.* **2016**, *112*, 1040–1048. [CrossRef]
26. Song, C.; Chung, J.; Kim, J.; Oh, J. Design optimization of a drifter using the Taguchi method for efficient percussion drilling. *J. Mech. Sci. Technol.* **2017**, *31*, 1797–1803. [CrossRef]
27. Kilickap, E. Determination of optimum parameters on delamination in drilling of GFRP composites by Taguchi method. *Indian J. Eng. Mater. S* **2010**, *17*, 265–274.
28. Song, C.; Kwon, K.; Park, J.; Oh, J.; Lee, S.; Shin, D.; Cho, J. Optimum Design of the Internal Flushing Channel of a Drill Bit using RSM and CFD Simulation. *Int. J. Precis Eng. Man.* **2014**, *15*, 1041–1050. [CrossRef]
29. Zhou, L.; Shi, W.; Wu, S. Performance Optimization in a Centrifugal Pump Impeller by Orthogonal Experiment and Numerical Simulation. *Adv. Mech. Eng.* **2013**, *5*, 385809. [CrossRef]
30. Gong, G.; Xu, C.; Jiao, J.; Liu, Y.; Xie, S. Investigation of moisture condensation on papermaking plant envelopes in high humidity environment by orthogonal analysis and CFD simulation. *Build. Environ.* **2011**, *46*, 1639–1648. [CrossRef]
31. Derdour, F.Z.; Kezzar, M.; Khochemane, L. Optimization of penetration rate in rotary percussive drilling using two techniques: Taguchi analysis and response surface methodology (RMS). *Powder Technol.* **2018**, *339*, 846–853. [CrossRef]
32. Vankanti, V.K.; Ganta, V. Optimization of process parameters in drilling of GFRP composite using Taguchi method. *J. Mater. Res. Technol.* **2014**, *3*, 35–41. [CrossRef]